



ELSEVIER

Available online at [www.sciencedirect.com](http://www.sciencedirect.com)

SCIENCE @ DIRECT®

Oceanologica Acta 26 (2003) 473–486

OCEANOLOGICA  
ACTA  
International Journal  
of Oceanology

[www.elsevier.com/locate/oceact](http://www.elsevier.com/locate/oceact)

## Friction and mixing in the Faroe Bank Channel outflow

### Friction et mélange dans le courant de sortie du chenal du banc des Faroe

Louise M. Duncan \*, Harry L. Bryden, Stuart A. Cunningham

*Southampton Oceanography Centre, Southampton SO14 3ZH, UK*

Received 29 July 2002; received in revised form 10 March 2003; accepted 24 March 2003

#### Abstract

Three hydrographic sections made during RRS *Discovery* cruise 242, from 7 September to 6 October 1999, are used to study the Faroe Bank Channel overflow. Each section, made perpendicular to the plume direction, comprised 10–14 stations measuring the outflow properties and velocity. The overflow defined as water with potential temperatures below 3 °C has densities greater than 28.1 kg m<sup>-3</sup>, salinities between 34.9 and 35.1, with velocities as high as 80 cm s<sup>-1</sup> approximately 20 km downstream from the sill. We use these measurements to describe the characteristics of the outflow and to estimate the amount of friction and mixing as the plume travels along the continental slope into the Iceland Basin. From Lowered Acoustic Doppler Current Profiler (LADCP) measurements we estimate stress in the bottom Ekman layer. Our stress results are best related to the overflow velocity with a drag coefficient of 0.5 × 10<sup>-3</sup> and to the height of the bottom Ekman layer with a von Karman constant of 0.75. Below a potential temperature of 8 °C, the isotherms sink with distance downstream. Calculating transport below different isotherms, we make an estimate for the amount of entrainment. In the region downstream of the sill, entrainment is initially maximum near the 0 °C isotherm just above the cold dense outflow and turbulent diffusivities reach as high as 500 cm<sup>2</sup> s<sup>-1</sup>. Fifty kilometre downstream of the sill the depth of maximum entrainment has moved upwards to the 2 °C isotherm and turbulent diffusivity has decreased to 50 cm<sup>2</sup> s<sup>-1</sup>. Froude numbers are found to exceed one in the centre of the overflow on all three sections. Calculating Richardson numbers we see evidence that mixing takes place above the fast flowing outflow core.

© 2003 Éditions scientifique et médicales Elsevier SAS and Ifremer/CNRS/IRD. All rights reserved.

#### Résumé

Trois sections hydrographiques réalisées durant la campagne 242 du R/V *Discovery*, du 7 septembre au 6 octobre 2002, sont utilisées pour étudier le flux de débordement du chenal du banc des Faroe. Chaque section perpendiculaire à la direction de propagation du panache comprend de 10 à 14 stations de mesurant les propriétés et de la vitesse du flux sortant. Le flux superficiel, défini comme une eau dont la température potentielle est inférieure à 3 °C, présente des densités supérieures à 28,1 kg m<sup>-3</sup>, des salinités entre 34,9 et 35,1 et des vitesses aussi élevées que 80 cm s<sup>-1</sup> approximativement sur 20 kilomètres en aval du seuil. Ces mesures permettent de décrire les caractéristiques du flux sortant et d'estimer la contribution de la friction et du mélange lorsque le panache se déplace le long de la pente continentale vers le bassin d'Islande. Des profils de courants basés sur des mesures LADCP permettent d'estimer le frottement dans la couche d'Ekman de fond. Ces résultats se relient aisément à la vitesse du flux sortant avec un coefficient de traînée de 0,5 10<sup>-3</sup> et à la hauteur de la couche de fond d'Ekman avec une constante de von Karman de 0,75. En-dessous d'une température potentielle de 8 °C, les isothermes plongent en même temps que le courant descendant. Le calcul de transport en dessous de différentes isothermes permet d'estimer la quantité entraînée. Dans la région en aval du seuil, l'entraînement est d'abord maximum près de l'isotherme 0 °C juste au-dessus du flux sortant d'eau dense et froide ; la diffusion turbulente atteint des valeurs aussi élevées que 500 cm<sup>2</sup> s<sup>-1</sup>. À 50 kilomètres du seuil, la profondeur du maximum d'entraînement s'est déplacée vers le haut jusqu'à l'isotherme 2 °C et la diffusion turbulente a décré jusqu'à 50 cm<sup>2</sup> s<sup>-1</sup>. Les nombres de Froude dépassent un dans le centre du flux de débordement sur les trois sections. Le calcul du nombre de Richardson met que le mélange se produit au-dessus du cœur rapide du flux sortant.

© 2003 Éditions scientifiques et médicales Elsevier SAS and Ifremer/CNRS/IRD. All rights reserved.

*Keywords:* Faroe Bank Channel; Overflow; Friction; Mixing

*Mots clés :* Chenal du banc des Faroe ; Flux supérieur ; Friction ; Mélange

\* Corresponding author.

E-mail address: [l.duncan@soc.soton.ac.uk](mailto:l.duncan@soc.soton.ac.uk) (L.M. Duncan).

## 1. Introduction

The Faroe Bank Channel is the deepest channel by which cold, dense Norwegian sea water overflows into the Iceland Basin, eventually going on to form part of the North Atlantic Deep Water (Saunders, 2001). With a maximum sill depth of 840 m, it has been estimated that 2 Sv of water overflows the Faroe Bank Channel with temperatures below 3 °C (Saunders, 1990). Recently, Hansen et al. (2001) noted a decrease in the pure Faroe Bank Channel outflow, colder than 0.3 °C, from 1.5 Sv in 1996 to 1.3 Sv in 1999. Although the amount of overflow through the Faroe Bank Channel sill is well established, there are still questions regarding the amount of friction and entrainment taking place downstream from the sill. Understanding the physics of such descending outflow plumes is fundamental for improving the parameterisation of these processes in current numerical models. As part of the Atlantic–Norwegian Exchanges (ANE) cruise, in September 1999, a study was carried out on the outflow from the Faroe Bank Channel.

A number of observations have previously been made on the Faroe Bank Channel outflow. In the late 1980s, two cruises studied the overflow using six moorings instrumented with current metres at approximately 5 km spacing (Saunders, 1990). Using these moorings together with hydrographic and shipboard Acoustic Doppler Current Profiler (ADCP) measurements, Saunders (1990) determined overflow speeds through the Faroe Bank Channel up to 1 m s<sup>-1</sup> with effective diffusivities near 100 cm<sup>2</sup> s<sup>-1</sup>. In 1995, Hansen et al. (2001) deployed a moored upward looking ADCP at the sill, which has provided a transport estimate below 3 °C of 1.9 Sv, consistent with that of Saunders (1990). Johnson and Sanford (1992) collected data from three expendable current profilers (XCP) drops and a (Conductivity, Temperature and Depth) CTD station in the centre of the sill in 1982. They analysed the vertical structure of the overflow and recorded an Ekman layer and found a logarithmic layer within the bottom boundary layer.

To date, there has been little progress published on the observations of physical processes acting on the Faroe Bank Channel overflow. However, in 1999 on RRS *Discovery*, sections were made across the overflow plume which combined CTD and Lowered Acoustic Doppler Current Profile (LADCP) observations on each station. These stations measure the high resolution horizontal and vertical structure of the overflow which enable a detailed analysis of the near bottom flow and a description of how the overflow evolves downstream of the sill. The sections provide higher spatial resolution compared with previous experiments. From these sections, estimates of the amount of friction and entrainment in the overflow are made as it flowed along and down the continental slope.

As an outline to this paper, Section 2 describes the data collection; initial observations of the overflow are then provided in Sections 3.1 and 3.2, followed by a description of the methods and results in calculating friction in Section 3.3.

There are comparisons with results from Armi (1977) and Killworth (2001) on overflow properties in Sections 3.4 and 3.5 followed by a study of mixing in Section 3.6. A final discussion is made in Section 4.

## 2. Materials and methods

The ANE cruise took place from 7 September to 6 October 1999, on board RRS *Discovery* as part of cruise D242 (Cunningham, 2000). Five LADCP/CTD sections were made perpendicular to the bathymetry of the Faroe Bank Channel, in and downstream from the sill at horizontal separations between 15 and 40 km. These sections, completed within 5 days of each other, are shown in Fig. 1.

One section is a repeat of section P, the first section downstream from the sill. Due to a beam failure on the LADCP during the first half of section P and all the Faroe Bank sill section, most of the current profiles were lost in these sections. Hence here we consider the three hydrographic sections: FBC, the second P section and section Q. In total 14 stations were occupied along section Q and 11 stations on the sections FBC and P. However only 10 stations make up our section P, as there are no LADCP data for the first shallowest station in this section.

All hydrographic stations used a Neil Brown Mark III CTD. CTD data were captured by the Southampton Oceanography Centre Data Acquisition Processing Software (SOC DAPS) and averaged into one-second data. Water samples were collected using a 24-bottle rosette for calibration of the CTD conductivity and to measure the concentration of silicon, nitrate, phosphate and dissolved oxygen.

Underway observations included meteorological, navigational and ADCP measurements. The shipboard RDI 150 kHz broadband ADCP measured currents to a depth of approximately 400 m, in 2 min averaged ensembles, in up to 64 8 m bins. ADCP headings were corrected using the onboard Ashtech GPS ADU (Global Positioning System Attitude Determination Unit).

For each section discussed, different LADCP instruments were used to provide full depth direct velocity measurements. The SOC 30° beam instrument was used on section FBC, the SOC 20° beam instrument on section P and the WHOI 30° beam instrument on section Q. Velocity data were collected in 2 min ensembles, in 10 × 16 m bins. The blank beyond transmit was set to 16 m, and bottom tracking was collected over the deepest 250 m in 16 m bins.

LADCP data were processed at sea using software from the University of Hawaii ADCP group. It extracted LADCP data into 5 m bins, removing those signals which would be contaminated by bottom echoes (dependent on beam angle), and combining it with the CTD and shipboard navigation to give absolute velocities from top to bottom with an uncertainty of 5 cm s<sup>-1</sup>.

During cruise *Discovery* 242, we also used a novel deep towed vehicle BRIDGET (British Mid–Ocean Ridge Initiative Towed vehicle), carrying two LADCPs, CTD and water

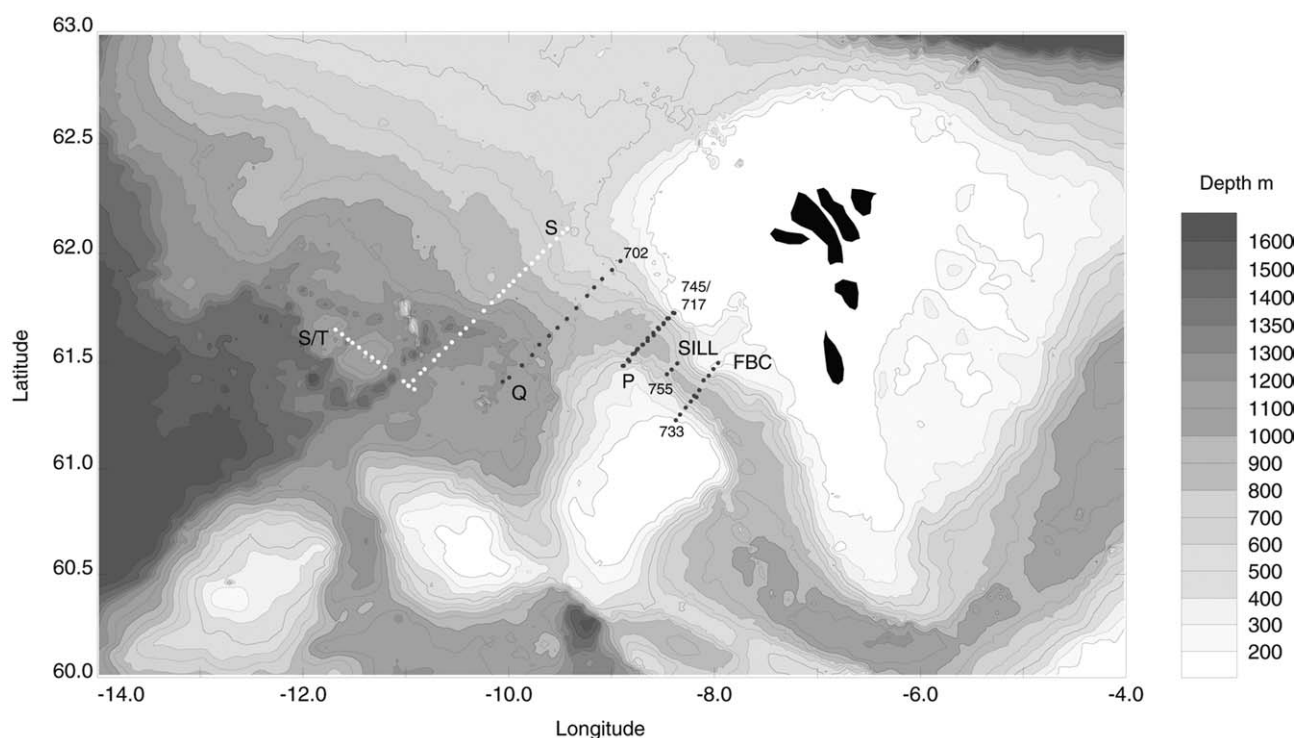


Fig. 1. Bathymetry near the Faroe Bank Channel with hydrographic sections made during cruise RRS *Discovery* 242. Black dots indicate CTD/LADCP stations and white dots indicate XBT positions on Bridget tow sections. Bathymetry is from the satellite derived bathymetry, version 8.2, of Smith and Sandwell (1997).

bottles, to make hydrographic and current measurements along three sections, perpendicular to the overflow plume. Although the operation and full analysis of these data are not discussed in detail in this paper, we will use results from BRIDGET section S, completed 40 km downstream from section Q, and section S/T, completed almost perpendicular to the southern end of section S, when discussing the path of the outflow plume. Our analysis of mixing in section 3.6 and discussions on the outflow path will also make use of XBT measurements along BRIDGET tow section S. In this paper, however, our primary attention will be on the LADCP/CTD stations in sections FBC, P and Q with overflow characteristics from these data described in Section 3.

### 3. Results

#### 3.1. Overflow characteristics

The LADCP measurements recorded profiles for the up and down casts. In the post-cruise processing, these profiles were averaged into 5 m bins, which were combined together to produce one velocity–depth profile for each cast. These profiles were merged onto CTD depth, temperature, salinity and potential temperature and rotated into along-track and across-track velocities. The rotations were  $136^\circ$ ,  $144^\circ$  and  $137^\circ$  for sections Q, FBC and P, respectively. Velocity and potential temperature contours are shown in Fig. 2. Positive velocities indicate north westward flow.

Within the Faroe Bank Channel section, the core is seen at a depth of 550–800 m. The outflow, water colder than  $3^\circ\text{C}$ , at

this point is confined by the channel bathymetry which keeps the core width at approximately 10 km. Most of the outflow has a temperature below  $0^\circ\text{C}$ , with maximum velocities up to  $70\text{ cm s}^{-1}$ . The overflow has salinities less than  $34.95$  and densities greater than  $28.1\text{ kg m}^{-3}$ . Further downstream at section P, the core is seen banked up on the northern slope as expected for geostrophic flow, and the overflow has deepened by 50 m to depths of 600–850 m. Overflow water is still confined within a channel, allowing the width to increase only slightly. Between the Faroe Bank Channel section and section P, the quantity of water with temperatures below  $0^\circ\text{C}$  has dropped by almost half indicating mixing and entrainment have taken place with the warmer, saltier water above. The maximum velocities in section P are  $80\text{ cm s}^{-1}$ ,  $10\text{ cm s}^{-1}$  faster than in the channel at the FBC section. Finally, reaching section Q, the outflow core reaches maximum speeds of  $70\text{ cm s}^{-1}$  and has increased its depth to 650–950 m. The width of the outflow has also doubled to 30 km since section P. This increase follows from the unbounded bathymetry of section Q. The core is still seen banked up on the northern slope in this final section. Transport of waters colder than  $0^\circ\text{C}$  in section Q is less than section P.

As previously mentioned these observations were made over several days. It has been reported that there may be fluctuations in the Faroe Bank Channel outflow, on time-scales of 3–4 days, causing the outflow temperature and currents to change by as much as  $3^\circ\text{C}$  and  $50\text{ cm s}^{-1}$ , respectively (Hoyer and Quadfasel, 2001). Our outflow speeds are low, as compared with Hansen et al. (2001) who see maximum velocities over  $100\text{ cm s}^{-1}$ . However, our

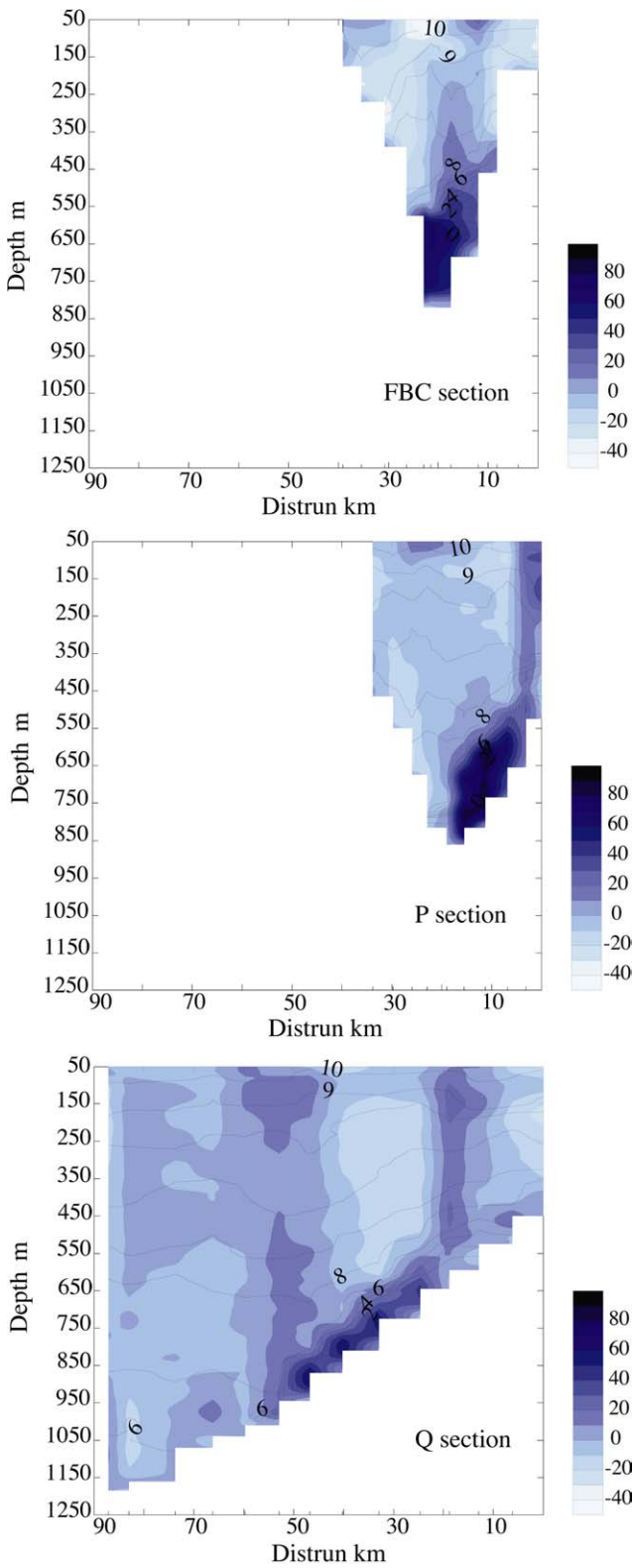


Fig. 2. Velocity ( $\text{cm s}^{-1}$ ) and temperature ( $^{\circ}\text{C}$ ) contours for sections FBC, P and Q from CTD/LADCP data. Velocities have been rotated to provide the across-track component with positive velocities indicating northwestward flow. The rotations were  $136^{\circ}$ ,  $144^{\circ}$  and  $137^{\circ}$  for sections Q, FBC and P, respectively. The Faroe Bank Channel overflow is seen in each section as cold, deep, fast flowing water.

maximum outflow velocities are in agreement with measurements by Johnson and Sanford (1992) and Saunders (1990). The fact that our transport estimates for all three sections are nearly the same suggests that time variability was not too great during the 5 days period.

3.2. Descent and spreading along the continental slope

The Faroe Bank Channel overflow spreads and deepens as it travels downstream from the sill along the continental slope (Fig. 2). Height and width definitions for the overflow can be made in two ways; using waters colder than  $3^{\circ}\text{C}$  or using salinity and temperature profiles where a well mixed layer is exhibited just above the bottom (Fig. 3). With these definitions, the mean height of the overflow for each section was obtained from stations where evidence of the overflow appeared (Fig. 4). For each section, the dashed lines show the maximum and minimum heights of the overflow. Heights were determined from the top of the overflow to the corrected

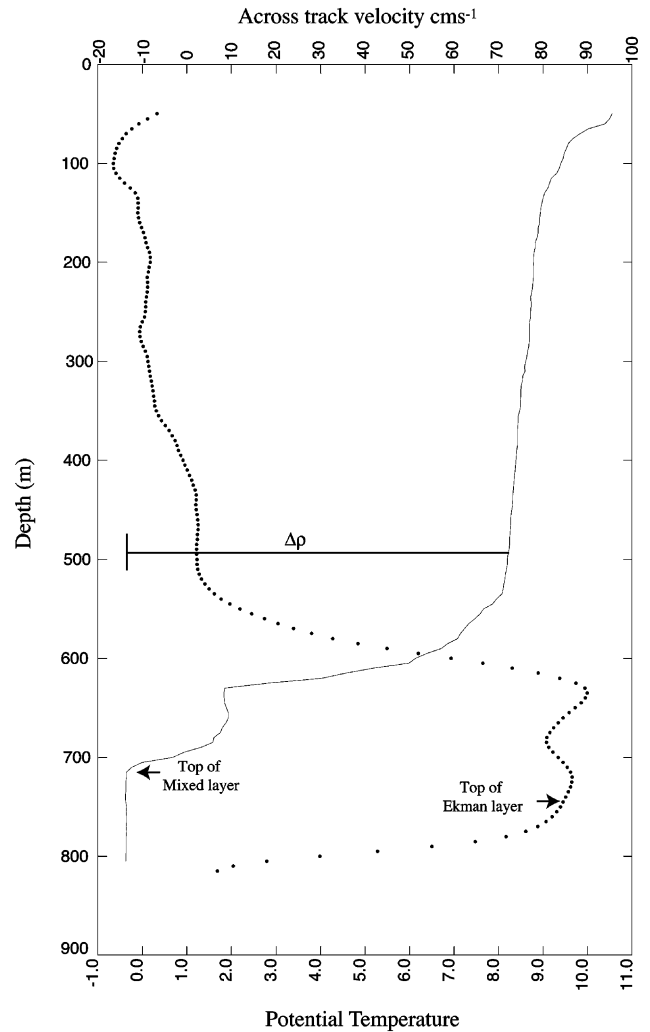


Fig. 3. A profile of across-track velocity (dotted line) and potential temperature (smooth line) for station 748 in section P. The height of the mixed layer and the Ekman layer are clearly seen in the temperature and velocity profiles respectively.

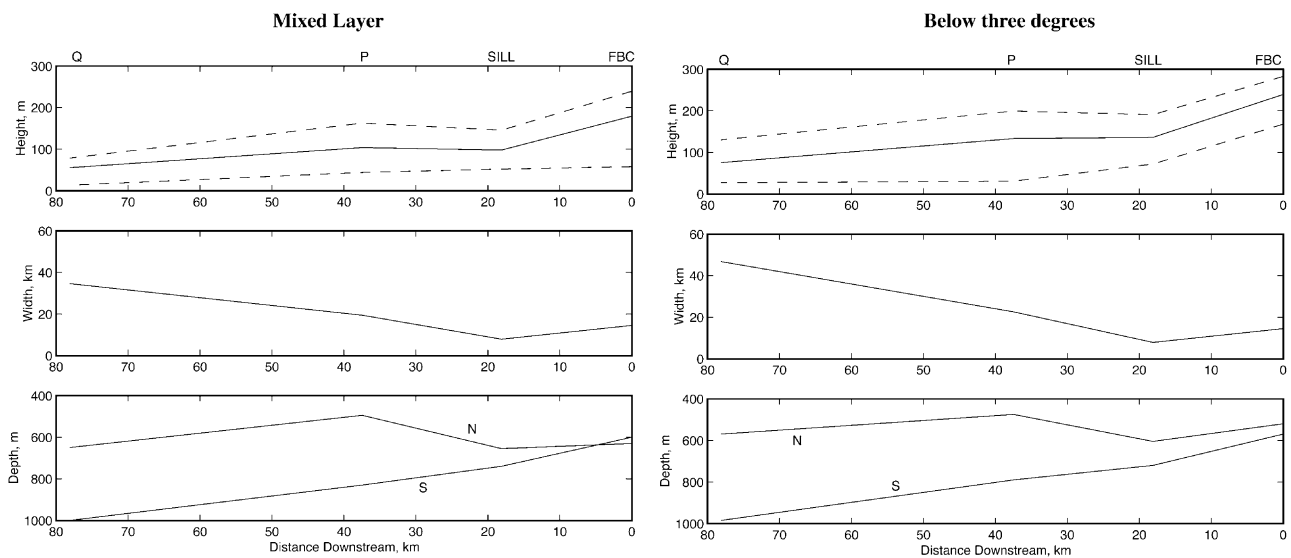


Fig. 4. The height, width and depth of the Faroe Bank Channel outflow. Two definitions for the outflow are used: water in mixed layer, defined from CTD temperature and salinity profiles, and water below the 3 °C isotherm. The mean height of the overflow for each section is determined from stations where the overflow appeared. The dashed lines give the maximum and minimum overflow heights along the section. The width is determined from the distance between those stations which have evidence of overflow plus half the distance to adjoining stations. Finally, the depths of the northern and southern edges of the overflow are determined from the stations farthest north and farthest south, respectively, with evidence of outflow water in them.

bottom depth, assuming the outflow made up the rest of the water depth. The width is defined as the distance between the stations with overflow water plus half the distance to neighbouring stations. Finally, the depth of the overflow on the northern and southern edges of the sections shows how the overflow thins from north to south.

The changes in these overflow properties over distance downstream are comparable with both definitions. The overflow is clearly seen to increase in width from approximately 10 km in the Faroe Bank Channel to 40 km at section Q. The depth increases both on the northern and southern edge of the outflows. However, the outflow has a much more rapid descent on the southern edge deepening by 400 m from a starting depth of 600 m in 80 km downstream. The northern edge is nearly level between the FBC section and the sill section, but it then shallows up to section P, before finally descending to section Q. The final depth change along the northern edge is only around 50 m in the total 80 km downstream. The outflow heights indicate that the thickest overflow is at the FBC section, with a general thinning downstream apart from a slight increase at section P. The overall patterns for the two definitions are very similar.

### 3.3. Friction

An important process acting on an outflow plume is the amount of bottom friction. In the bottom layer, the outflow is acted on by bottom stresses, which create an Ekman layer and associated cross channel flow. To determine the amount of bottom stress in the bottom Ekman layer, our velocity profiles were first extended to reach as close to the bottom as possible. In the usual LADCP processing, velocity profiles are clipped near the bottom due to the possibility of contaminated signals from bottom echoes. The amount of clipping

depends on the angle of the LADCP beam. In our processing, we do not clip the velocity data so as to extend our profiles as deep as possible.

The bottom Ekman layer appears in velocity profiles as a spiral, like that shown in Fig. 5, for station 707 from section Q. In order to determine the amount of bottom friction, the near bottom LADCP measurements for stations across FBC, P and Q were used. Clean spirals, like Fig. 5, are only seen in fast velocity stations, but estimates of bottom friction were made for all stations in each section. Before using the newly extended velocity profiles for stress calculations, the profiles in strong currents were carefully compared with Vessel

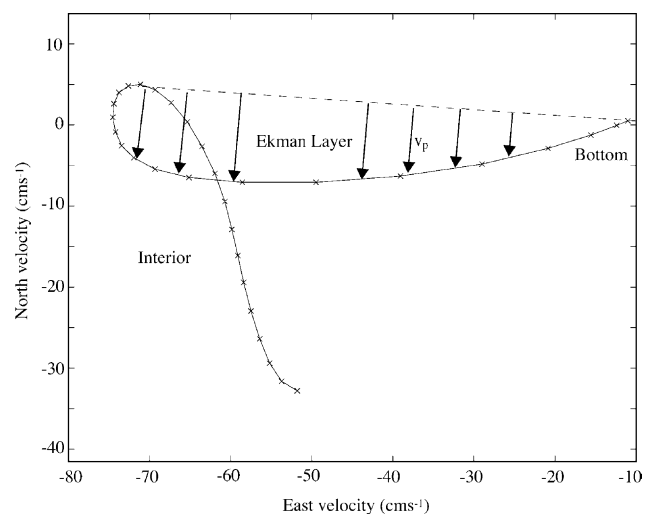


Fig. 5. An Ekman spiral seen from LADCP data on station 707 in section Q. Vertical integration of the perpendicular velocity, shown by the black arrows, to the principal plume direction, shown by dashed line, in the Ekman layer provides an estimate of bottom stress. The crosses indicate measurements at 5 m depth intervals.

Mounted ADCP (VMADCP) and bottom tracking from LADCP profiles to choose a single barotropic velocity adjustment for each profile.

The bottom Ekman layer is a region of non-constant stress. Determination of bottom friction in this non-constant stress region can be made by estimating the flow perpendicular to the principal orientation of the plume velocity. (The principal orientation of the flow is the direction the flow would have if there were no bottom friction effects). The dashed line in Fig. 5 shows the principal orientation of the flow and the dark arrows indicate the perpendicular flow,  $v_p$ . Vertical integration of this perpendicular velocity,  $v_p$ , provides estimates of bottom stress,  $\tau = \rho f \int v_p dz$ .

In calculating bottom friction, we determined the principal plume direction from velocity hodographs. The direction of the principal plume was taken as the direction between the bottom most velocity point and the point of maximum speed. Maximum speed occurs at the end of the spiral and hence the top of the Ekman layer. Results are shown in Table 1 for sections FBC, P and Q. The table also presents maximum plume speeds, direction, and depth of the Ekman layer and stress values. The italicised stations are considered to be within the main overflow path. They contain the fastest velocities, deepest Ekman layers and highest bottom stresses.

### 3.4. Theories for the bottom Ekman layer

A discussion of bottom boundary layers over the Hatteras Abyssal Plain by Armi (1977) utilised theories of a turbulent Ekman layer on a flat bottom to determine Ekman layer height. We use the relations given by Armi to see how well our results compare with standard predictions (Fig. 6).

In particular, we examine two relations. Firstly, between the height of the Ekman layer and the bottom stress

$$h_e = ku_* / f \quad (1)$$

where  $h_e$  is the height of the turbulent Ekman layer,  $f$  is the Coriolis parameter,  $u_*$  is friction velocity equal to  $(\tau/\rho)^{1/2}$  and  $k$  is the von Karman constant usually taken to equal 0.4. Secondly, there is a relation between the stress and the speed of the outflow

$$\tau = \rho c_D U^2 \quad (2)$$

where  $\tau = \rho u_*^2$ ,  $U$  is the maximum speed and  $c_D$  is the drag coefficient.

Using the estimates of these properties from all our LADCP sections where the frictional stress is positive and taking  $f$  to be  $1.3 \times 10^{-4} \text{ s}^{-1}$ , our results agree reasonably well with Armi. Higher stress values are related both to higher Ekman speeds and thicker Ekman layers. Plotting stress vs. Ekman layer height (Fig. 6a) we find the best fit occurs for  $k$  equal to 0.75 compared with a standard value of 0.4. Plotting stress vs. outflow speed (Fig. 6b) we find the best fit occurs for  $c_D$  equal to  $0.47 \times 10^{-3}$  compared with a standard value of  $2.5 \times 10^{-3}$ .

In Armi (1977) the bottom Ekman layer was found to lie within the bottom mixed layer. In Fig. 3, the Ekman layer makes up approximately 70% of the bottom mixed layer

depth. However, most of the stations show an Ekman layer depth greater than the mixed layer depth (Table 1), a result inconsistent with that of Armi (1977).

### 3.5. Path of the outflow plume

By taking the maximum plume velocity, which is above the bottom boundary region of frictional influence, Fig. 7 shows the velocity vectors for each station in sections FBC, P and Q in black. The gray vectors are those from absolute velocities from Bridget at a depth of 64 m off the bottom, averaged over 20 min, which corresponds to a horizontal resolution of 1.8 km. The flow closely follows the isobaths at sections FBC and P with headings of 140–150°, but there is a significant downslope flow on the southern side of section Q. The BRIDGET section S, displays the flow following the isobaths in the northern part with a possible indication of downslope flow in the middle and southern parts of the section. Section S/T indicates fast south westward flow on the southern part of the section through a deeper channel. It has been previously mentioned that a branch of the main overflow may descend directly into the Iceland Basin through such a deeper channel (Hansen and Østerhus, 2000). Observations by Duncan et al. (2002) support this view, determining the coldest temperature of the fast flow at S/T to be 1.1 °C.

There is an argument that a plume should fall across depth contours by 1 in 400, independent of frictional effects (Killworth, 2001). For standard plume models this descent rate is equivalent to  $c_D^{-1}$ , so 1 in 400 is equivalent to a  $c_D$  of  $2.5 \times 10^{-3}$  (Kase, personal communication). To test this hypothesis, contour plots of each isotherm for sections FBC, P, Q and S were made and a linear fit was determined for each isotherm to find its slope across the section and the mean height at each section (Table 2).

It is clear that in all cases the isotherms are sinking as the distance increases away from the Faroe Bank Channel section. In general, the isotherms slope from north to south with only two exceptions both occurring in the FBC section on the 0 and 1° isotherms, as seen in Fig. 2. Taking the distance between sections as approximately 37.1, 44.2 and 39.1 km for FBC–P, P–Q and Q–S, respectively, estimates can be made of the sinking rate of the plume. To overcome the difference in section widths, we initially centred the isotherms to lie above each other before the calculation. We find the plume falls at various rates between 1 in 250 and 1 in 1340 between sections, depending on the isotherm. Fig. 8 shows the sinking 3 °C isotherm. Between the FBC section and section P all the isotherms for 3 °C and below fall between 1 in 250 and 1 in 445. These results agree well with Killworth (2001). For sections P and Q the plume falls more gradually at rates between 1 in 500 and 1 in 800 (ignoring our result for the 1 °C isotherm of 1 in 1340). The fall rate has halved between these sections suggesting that  $c_D$  has approximately halved to about  $1.25 \times 10^{-3}$ . The reason for this slow down in fall rate could be attributed to the thinning and spreading of the plume below the 3° isotherm downstream

Table 1

Stress estimates determined from velocity hodographs at each station on sections FBC, P and Q. The speed and principal plume direction is determined at the top of the Ekman layer. Stress is determined by the vertical integration of the perpendicular velocity to the principal plume direction. The stress + 5 and stress – 5 are stress results for 5 m above and below our chosen Ekman layer height. Bold stations are within the main overflow

Station	Depth (m)	Speed (cm s <sup>-1</sup> )	Direct (of max. velocity)	Ekman layer depth (m)	CTD mixed layer (m)	Stress (N m <sup>-2</sup> )	Stress + 5 (N m <sup>-2</sup> )	Stress – 5 (N m <sup>-2</sup> )
<i>FBC section</i>								
North								
743	199	26	302	44	17	-0.3	-0.7	-0.1
742	189	28	311	69	22	-1.5	-2.2	-1.0
741	462	20	132	32	12	0.2	0.3	0.1
740	<b>688</b>	<b>47</b>	<b>194</b>	<b>78</b>	<b>25</b>	<b>-2.2</b>	<b>-2.7</b>	<b>-1.5</b>
739	<b>828</b>	<b>51</b>	<b>153</b>	<b>93</b>	<b>68</b>	<b>1.5</b>	<b>1.9</b>	<b>1.1</b>
738	<b>823</b>	<b>68</b>	<b>150</b>	<b>98</b>	<b>202</b>	<b>2.7</b>	<b>2.5</b>	<b>2.7</b>
737	<b>839</b>	<b>60</b>	<b>147</b>	<b>104</b>	<b>241</b>	<b>4.3</b>	<b>4.8</b>	<b>3.7</b>
736	577	22	269	82	26	-1.1	-1.3	-0.9
735	394	32	317	84	21	-2.3	-2.9	-1.8
734	275	61	24	55	16	0.0	-0.2	0.2
733	179	27	66	49	23	0.1	0.3	0.1
South								
<i>P section</i>								
North								
745	537	15	31	47	20	0.2	0.2	0.1
746	658	20	116	33	14	0.1	0.2	0.0
747	<b>738</b>	<b>39</b>	<b>120</b>	<b>38</b>	<b>23</b>	<b>0.6</b>	<b>0.7</b>	<b>0.5</b>
748	<b>825</b>	<b>85</b>	<b>139</b>	<b>80</b>	<b>112</b>	<b>1.8</b>	<b>2.3</b>	<b>1.5</b>
749	<b>874</b>	<b>81</b>	<b>132</b>	<b>54</b>	<b>23</b>	<b>1.2</b>	<b>1.8</b>	<b>0.9</b>
750	874	9	208	<b>59</b>	<b>37</b>	<b>1.4</b>	<b>1.9</b>	<b>0.9</b>
751	821	22	18	76	13	-2.7	-2.5	-2.7
752	686	30	358	76	50	-0.4	-0.4	-0.4
753	550	22	13	45	15	-0.6	-0.9	-0.3
754	471	12	39	51	20	0.9	0.8	0.8
South								
<i>Q section</i>								
North								
702	452	42	215	52	19	0.7	0.1	1.0
703	530	4	238	25	14	0.0	0.2	0.0
704	597	11	9	47	18	-2.5	-3.4	-1.7
705	649	12	51	49	21	-0.5	-0.7	-0.4
706	<b>729</b>	<b>59</b>	<b>180</b>	<b>79</b>	<b>79</b>	<b>0.6</b>	<b>0.6</b>	<b>0.5</b>
707	<b>815</b>	<b>73</b>	<b>176</b>	<b>85</b>	<b>55</b>	<b>6.0</b>	<b>6.2</b>	<b>5.4</b>
708	<b>873</b>	<b>91</b>	<b>185</b>	<b>73</b>	<b>67</b>	<b>5.3</b>	<b>5.3</b>	<b>5.0</b>
709	<b>957</b>	<b>92</b>	<b>185</b>	<b>82</b>	<b>63</b>	<b>2.7</b>	<b>2.7</b>	<b>2.4</b>
710	1013	28	160	33	14	0.9	1.8	0.4
711	1043	10	33	48	15	0.5	0.4	0.4
712	1071	3	278	21	20	0.0	-0.1	0.0
713	1163	9	214	28	20	0.1	0.1	0.0
714	1189	17	223	34	27	-0.5	-0.9	-0.3
715	1207	17	51	47	13	0.1	-0.1	0.3
South								

from the sill. Killworth (2001) assumes a slab like plume of constant height. In our observations, it is interesting to note that the 3 °C isotherm falls across depth contours in the middle and on the southern edge but does not cross depth contours on the northern edge.

### 3.6. Mixing

Knowledge of the final properties of the outflow after descending from the channel is vitally important if we are to understand how the initial North Atlantic Deep Water prop-

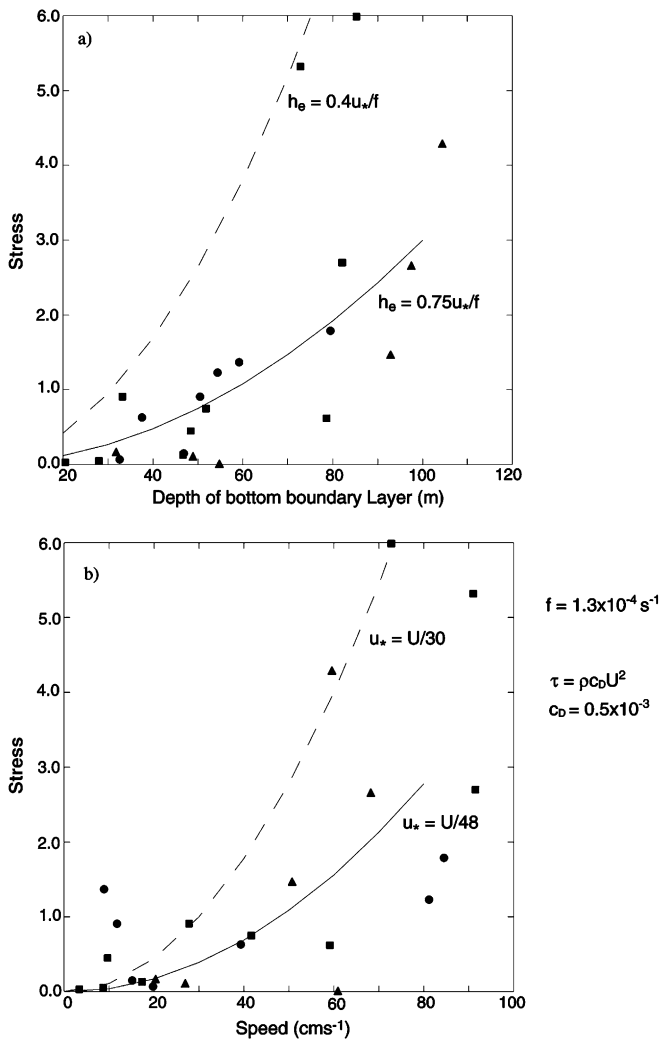


Fig. 6. Relationships between properties in the bottom Ekman Layer. (a) Stress ( $\tau = \rho u_*^2$ ) vs. the thickness of the bottom boundary layer,  $h_e$  and (b) stress vs. speed of the outflow,  $U$ . Solid lines indicate our best fit. Stations in the FBC, P and Q sections are represented by triangles circles and squares, respectively. Armi's (1997) results are shown by the dashed line.

erties are determined. We consider four methods of observing the amount of mixing taking place along the outflow path: transport in temperature classes, turbulent diffusivities, Froude numbers and Richardson numbers.

3.6.1. Separating into temperature classes

The amount of mixing taking place along the path of the Faroe Bank Channel overflow can be considered through the changes in transport for different temperature classes. To obtain transport estimates for a particular section, the 5 m LADCP velocities at each station are multiplied by half the distance to the adjacent stations, either side, at the same depth. For each of the two outermost stations at the end of each section, only half the distance to its only adjoining station is used. Near the bottom some stations extend deeper than their neighbouring stations. To account for this, linear interpolation between the bottom depth of neighbouring stations is used to calculate areas in this region. Matching the

LADCP depth with the CTD depth, we use the CTD potential temperature to divide transports into temperature classes. These are shown in Table 3 and Fig. 9 for temperature classes below 0 and 1 °C, to below 5 °C.

Table 3 shows that the amount of transport below each temperature class decreases as the distance downstream from the sill increases. Transport below the 3 °C isotherm declines from 1.60 to 1.24 Sv between the FBC section and Q section. These estimates of transport agree with previous estimates from Saunders (1990) and Hansen et al. (2001). Following a transport of 1.60 Sv from the FBC section downstream, we find that by section Q this same transport accounts for all water below 5 °C.

3.6.2. Turbulent diffusion rates

Developing the study of mixing along the Faroe Bank Channel outflow further, we estimate the turbulent diffusion rates across isotherms between each of our sections. Initially, we determined the height of each isotherm, from 0 to 5 °C, by averaging the height of individual isotherms on all stations making up each section. Combining these to give an average height for the section, the downward slope of each isotherm can be seen along the outflow path (Fig. 9) with the isotherm slope not approaching zero until we reach the 9 °C isotherm. The mean heights for section S were obtained using the same procedure as for CTD stations although replacing CTD data with XBT data, which were launched along the section approximately every 7.2 km. Using these estimates and the overflow transport between each isotherm, we build a picture of changes in transport (Fig. 9). A certain amount of cold Norwegian seawater flows through the Faroe Bank Channel; but since a lesser amount of this same temperature water crossing at section P or Q, some water has crossed the isotherm upward. Each of these amounts is indicated in Fig. 9 by the blue upward arrow. From these changes in transport below a given isotherm, turbulent diffusion rates can be determined using

$$Q_{in} T_{in} - Q_{out} T_{out} + (Q_{in} - Q_{out}) N^\circ C + K \frac{\partial T}{\partial z} \times \Delta x \Delta y = 0 \tag{3}$$

where the vertical temperature gradient is calculated at the  $N^\circ$  isotherm,  $\Delta x \Delta y$  is the area between the sections and  $T_{in}$ ,  $T_{out}$  are the velocity weighted temperatures of the water entering, leaving each section below the  $N^\circ$  isotherm. The vertical temperature gradient is determined by taking the temperature difference between the neighbouring isotherms divided by the difference in height between them. For the 0 °C isotherm, the difference between the -0.15 and 1 °C isotherm is used while all others are based on a difference over 2 °C. The distance downstream between sections is determined using station positions, where the average 0 °C isotherm height most closely matches the station. To determine an accurate single temperature value for water entering each section, we adapt the velocity-weighted method used by Baringer and Price (1997a, b). Replacing salinity with

### Outflow Speed and Direction For Sections S/T, S, P, FBC and Q

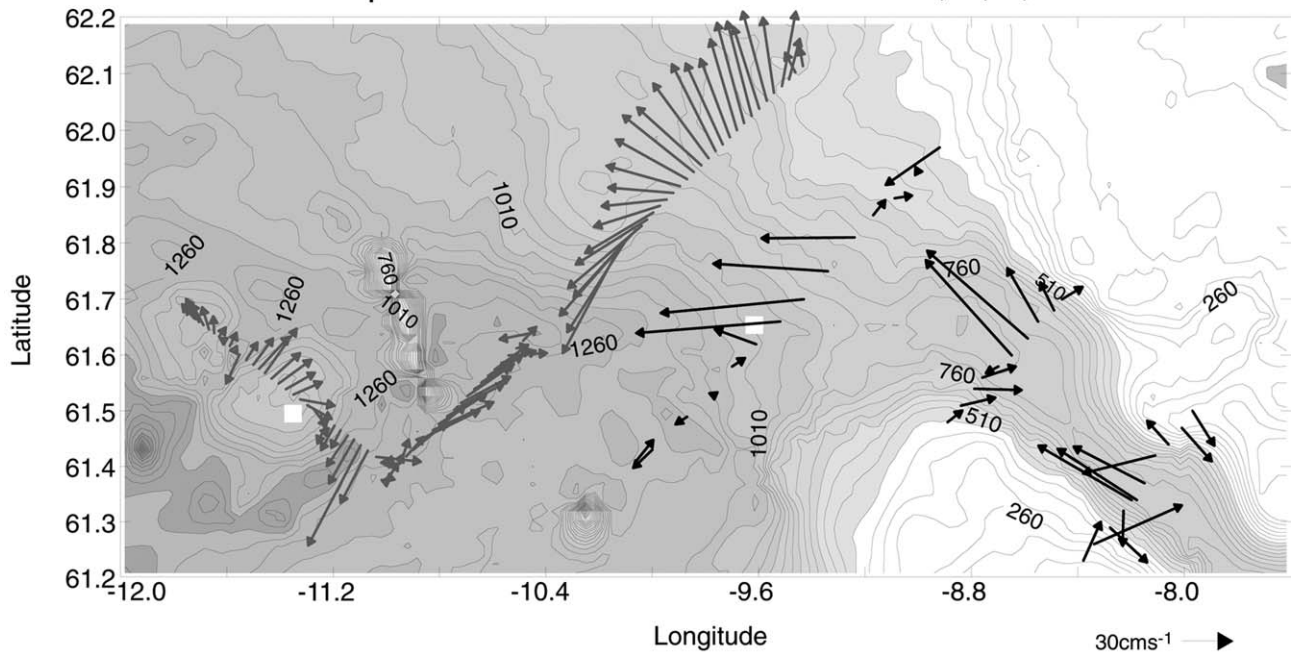


Fig. 7. Outflow speed and direction for sections FBC, P and Q are shown by black vectors, which represent the flow at the top of the Ekman layer. The gray vectors are data from the BRIDGET deep tow vehicle and are velocities at 64 m above the bottom, averaged over 20 min, that is separated by approximately 1.8 km.

Table 2

Estimates of sinking isotherms. The slope of the isotherms was determined at each section by fitting a linear polynomial to the station data. Mean depths were derived after isotherms had been centred, taking the mid point as the mean depth. For sections FBC, P and Q, CTD data were used in the calculations. For section S, XBT data are used. Approximate distances between sections, provided below the table, are used to estimate how much the isotherm sink downstream. Distance downstream is derived between the middle stations on each section

Isotherm (°C)	FBC		P		Q		S	
	Slope across section (m km <sup>-1</sup> )	Mean depth of isotherm (m)	Slope across section (m km <sup>-1</sup> )	Mean depth of isotherm (m)	Slope across section (m km <sup>-1</sup> )	Mean depth of isotherm (m)	Slope across section (m km <sup>-1</sup> )	Mean depth of isotherm (m)
0	-4.5	626	8.4	745	11.0	781	-	-
1	-0.4	592	11.1	715	11.2	772	-	-
2	2.5	570	15.9	670	12.7	768	10.2	1045
3	5.6	546	16.5	648	10.3	746	9.9	906
4	8.9	528	15.1	633	10.3	732	9.3	887
5	9.7	500	15.2	619	9.7	727	7.7	830
8	12.8	459	8.2	511	3.2	562	2.4	621

Distance between sections approximately

FBC–P	37.1 km
P–Q	44.2 km
Q–S	39.1 km

temperature in their Eq. (1), we resolve the velocity-weighted temperature for each station using

$$T_{vwtD} = \frac{\int_D^{D+h} T \vec{v} \cdot \vec{n} \, dz}{\int_D^{D+h} \vec{v} \cdot \vec{n} \, dz} \quad (4)$$

where  $n$  is the direction normal to the section,  $D$  is the bottom

depth and  $h$  is the depth of the  $N^\theta$  isotherm at that section. To average over each section, the temperature is

$$T_{in}, T_{out} = \frac{\int_0^W dy \int_D^{D+h} T \vec{v} \cdot \vec{n} \, dz}{\int_0^W dy \int_D^{D+h} \vec{v} \cdot \vec{n} \, dz} \quad (5)$$

where  $W$  is the width of the outflow. The definition of  $W$  is the

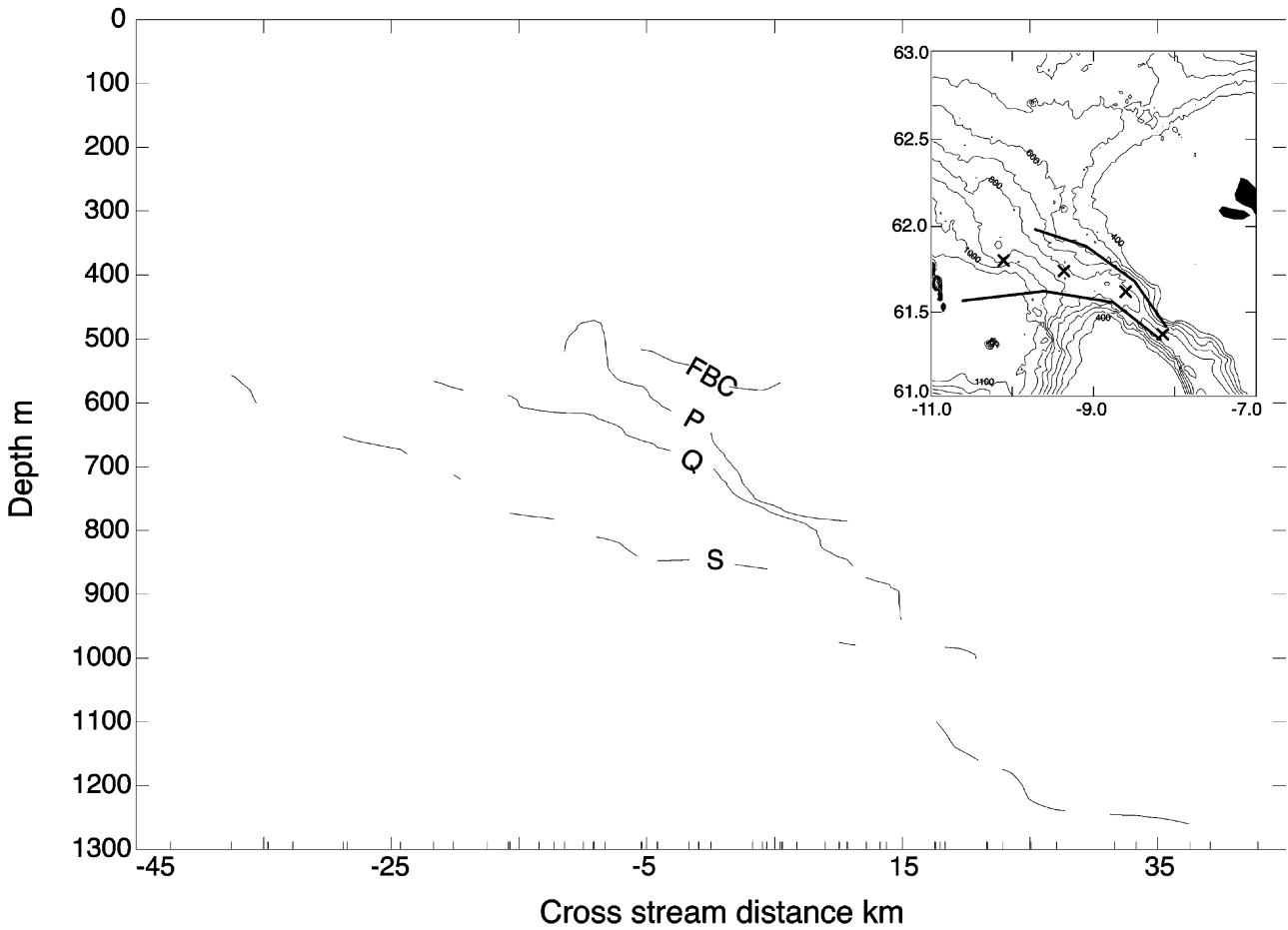


Fig. 8. Shape of the 3° isotherm for sections FBC, P, Q and S. Section S is an XBT and BRIDGET section. The isotherms are centred for comparison. The path of the 3° isotherm across bathymetry is shown in the top right-hand corner. Solid lines denote the upper and lower limits of the isotherm and the crosses indicate the centre of the isotherm at each section.

Table 3  
Overflow transport separated into temperature classes

Temperature (°C)	FBC section (Sv)	P section (Sv)	Q section (Sv)
<0	1.09	0.59	0.42
<1	1.32	0.92	0.89
<2	1.45	1.33	1.07
<3	1.60	1.46	1.24
<4	1.71	1.55	1.47
<5	1.78	1.71	1.60
<6	1.83	1.79	1.73
<7	1.87	1.93	1.93

same as that described for water below the 3 °C isotherm in Section 2, but using the appropriate N° isotherm for the calculation. The red downward arrows in Fig. 9 indicate the resulting *K* estimates.

According to our calculations, most mixing takes place between sections FBC and P with diffusion rates as high as 500 cm<sup>2</sup> s<sup>-1</sup>. Farther downstream between sections P and Q, rates decrease by an order of magnitude to about 50 cm<sup>2</sup> s<sup>-1</sup>. The higher rates between FBC and P are associated with

larger transports across isotherms, particularly below 2 °C, and to larger changes in temperature below isotherms, particularly those warmer than 2 °C, between these sections.

Previous estimates made with combined ADCP and CTD sections in spring 1987 and 1988 give turbulent diffusion rates at the 3 °C isotherm between 50 and 150 cm<sup>2</sup> s<sup>-1</sup> (Saunders, 1990). These were calculated over a region which encompasses our sections FBC to Q. Recalculating a turbulent diffusion rate over this region gives 144 cm<sup>2</sup> s<sup>-1</sup>, which is in agreement with Saunders (1990).

### 3.6.3. Froude numbers

The previous methods have indicated a high level of mixing between sections FBC and P, trailing off towards section Q. They have involved looking at section-averaged calculations. Using Froude numbers, we can observe variations in mixing along each section, which provide indications of entrainment rates by looking at the rate of flow of the overflow. The Froude number is given by

$$F = \frac{U^2}{g'H} \tag{6}$$

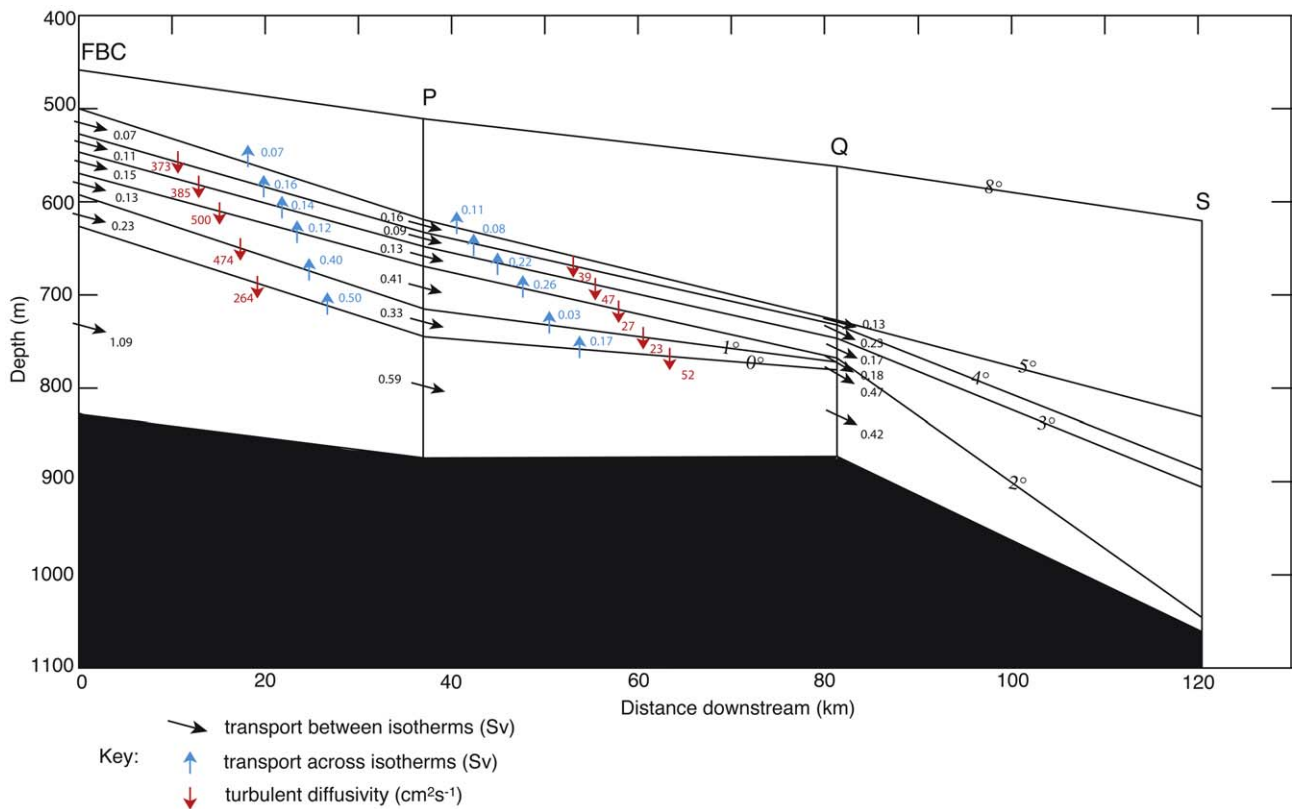


Fig. 9. A schematic for turbulent diffusion and entrainment in the Faroe Bank Channel outflow. Black arrows indicate plume transports between isotherms. The blue arrows provide the resulting transport across isotherms, between each section, and the red arrows show turbulent diffusion rates. Note the high diffusivity indicated between sections FBC and P.

where  $U$  is the speed of the overflow,  $H$  is the thickness of the overflow and  $g'$  is the reduced gravity, given by

$$g' = \frac{g(\rho_2 - \rho_1)}{\rho_2} \quad (7)$$

where  $\rho_1$  and  $\rho_2$  are the North Atlantic and overflow water densities, respectively. It is generally considered that the faster moving flow below a slower moving upper flow will start to entrain water from above when the Froude number is greater than or equal to one (Baringer and Price, 1997a).

Using speed estimates obtained from the study of the Ekman layer spirals and the CTD profiles, we calculate Froude numbers for each station. The densities are calculated using CTD temperature and salinity, and the heights of the mixed layer are determined from profiles of salinity and temperature (Fig. 3 and Table 1).

The regions where there are high stresses tend to coincide with higher Froude numbers (Tables 1 and 4). We obtain Froude numbers greater than one, reaching as high as 4.8, in the centre of the sections where the overflow appears (italicised parts of tables). Generally, low Froude numbers at the FBC section occur because the mixed layer is very deep. Since the FBC section is upstream of the sill, we expect subcritical flow there. Stations 737 and 738 both have mixed layer depths in excess of 200 m. At sections P and Q, Froude numbers are generally greater than one when the flow is

faster than  $40 \text{ cm s}^{-1}$ . The large Froude numbers occurring near the ends of each section are due to smaller mixed layer depths, likely related to edge effects.

### 3.6.4. Richardson numbers

Analysis of Froude numbers leads to an examination of Richardson numbers in section P. Ocean models often use Richardson numbers as initial conditions for mixing in flow over sills. It could therefore be beneficial to estimate these non-dimensional numbers to compare with model results. Richardson numbers provide a measure of the stability or instability of the flow and are calculated by dividing the buoyancy frequency ( $N$ ) squared, a measure of stability given by  $-g(\partial\rho/\partial z)/\rho$ , by the square of total velocity shear;

$$R_i = \frac{N^2}{\left(\frac{\partial u}{\partial z}\right)^2} \quad (8)$$

The critical value for Holmboe instability, a process where gravity and vorticity waves interact in highly sheared and stratified flows (Baines, 2001), occurs when the Richardson number is approximately a quarter. For gradient Richardson numbers less than one-quarter the current is unstable. Usually Richardson numbers are estimated over finite thickness, here we calculate velocity shear and  $N^2$  over 5 m scales. For

Table 4

Froude number estimates for all stations in sections FBC, P and Q. The speed is determined at the top of the Ekman layer and mixed layer depths and density differences from CTD data. Bold stations are within the main overflow

Station	Speed (ms <sup>-1</sup> )	Overflow density anomaly (kg m <sup>-3</sup> )	Upper layer density anomaly (kg m <sup>-3</sup> )	Density difference (kg m <sup>-3</sup> )	CTD mixed layer depth (m)	Froude number
<i>FBC section</i>						
North						
743	0.26	27.31	27.26	0.05	17	8.1
742	0.28	27.35	27.31	0.04	22	9.8
741	0.20	27.81	27.68	0.13	12	2.9
<b>740</b>	<b>0.47</b>	<b>28.03</b>	<b>27.41</b>	<b>0.62</b>	<b>25</b>	<b>1.5</b>
<b>739</b>	<b>0.51</b>	<b>28.06</b>	<b>27.45</b>	<b>0.61</b>	<b>68</b>	<b>0.7</b>
<b>738</b>	<b>0.68</b>	<b>28.06</b>	<b>27.43</b>	<b>0.63</b>	<b>202</b>	<b>0.4</b>
<b>737</b>	<b>0.60</b>	<b>28.06</b>	<b>27.43</b>	<b>0.63</b>	<b>241</b>	<b>0.3</b>
736	0.22	27.47	27.44	0.03	26	6.5
735	0.32	27.41	27.35	0.06	21	8.6
734	0.61	27.28	27.20	0.08	16	29.6
733	0.27	27.25	27.24	0.01	23	32.4
South						
<i>P section</i>						
North						
745	0.15	27.86	27.71	0.15	20	0.8
746	0.20	27.95	27.40	0.55	14	0.5
<b>747</b>	<b>0.39</b>	<b>28.01</b>	<b>27.43</b>	<b>0.58</b>	<b>23</b>	<b>1.2</b>
<b>748</b>	<b>0.85</b>	<b>28.05</b>	<b>27.43</b>	<b>0.62</b>	<b>112</b>	<b>1.1</b>
<b>749</b>	<b>0.81</b>	<b>28.05</b>	<b>27.43</b>	<b>0.62</b>	<b>23</b>	<b>4.8</b>
750	0.09	28.05	27.56	0.49	37	0.1
751	0.22	28.05	27.51	0.54	13	0.7
752	0.30	27.47	27.43	0.04	50	4.8
753	0.22	27.46	27.44	0.02	15	17.2
754	0.12	27.45	27.43	0.02	20	3.6
South						
<i>Q section</i>						
North						
702	0.42	27.59	27.54	0.05	19	18.7
703	0.04	27.75	27.45	0.30	14	0.0
704	0.11	27.91	27.68	0.23	18	0.3
705	0.12	27.93	27.44	0.49	21	0.2
<b>706</b>	<b>0.59</b>	<b>28.00</b>	<b>27.45</b>	<b>0.55</b>	<b>79</b>	<b>0.9</b>
<b>707</b>	<b>0.73</b>	<b>28.04</b>	<b>27.45</b>	<b>0.59</b>	<b>55</b>	<b>1.7</b>
<b>708</b>	<b>0.91</b>	<b>28.05</b>	<b>27.44</b>	<b>0.61</b>	<b>67</b>	<b>2.1</b>
<b>709</b>	<b>0.92</b>	<b>28.05</b>	<b>27.51</b>	<b>0.54</b>	<b>63</b>	<b>2.6</b>
710	0.28	28.02	27.62	0.40	14	1.4
711	0.10	27.63	27.45	0.18	15	0.4
712	0.03	27.64	27.44	0.20	20	0.0
713	0.09	27.69	27.48	0.21	20	0.2
714	0.17	27.70	27.62	0.08	27	1.3
715	0.17	27.70	27.65	0.05	13	4.9
South						

such bulk Richardson numbers, the flow is often considered to be unstable when  $R_i < 1$ .

Initially, the density and velocity gradients were determined over depth changes of 10 m, but we later changed to 5 m to enable a calculation over smaller depth intervals. Density is derived from the CTD temperature, pressure and salinity and velocities from the LADCP data, corrected against VMADCP and bottom track velocities.

The individual stations, for section P, are gridded to produce the contoured sections (Fig. 10). The Richardson numbers are shown by the shading overlaid on the velocity and temperature sections. Broad bands of Richardson numbers between 0–1, 1–3 and 3 and above are highlighted. This is due to the sensitivity of our Richardson numbers to depth scales and time averaging. The change to smaller vertical scales caused our Richardson number profiles to become less

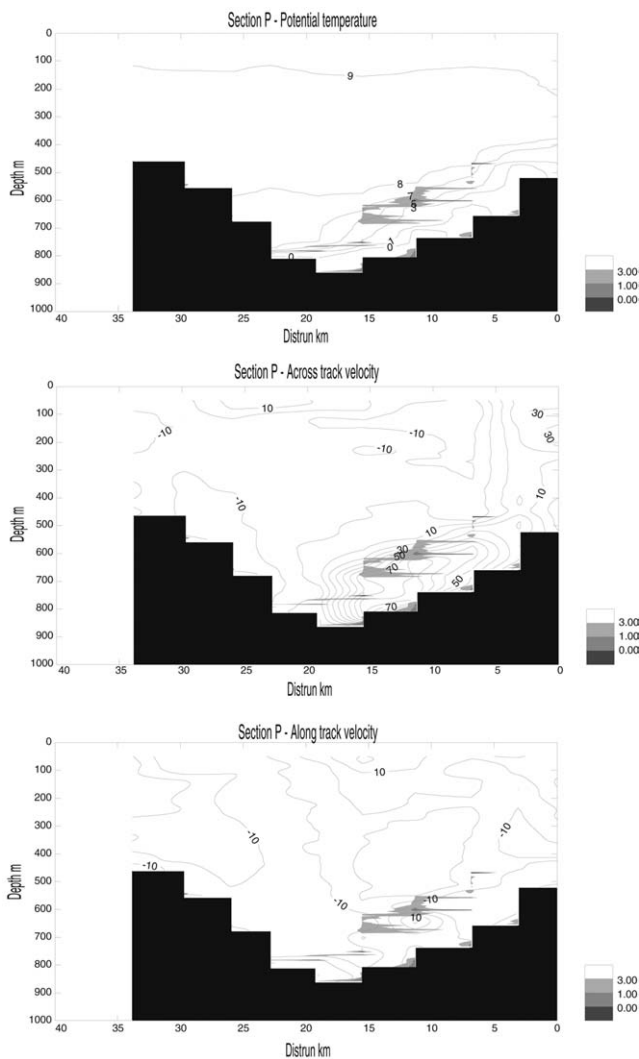


Fig. 10. Regions in section P where Richardson numbers are less than three exist together with (i) potential temperature contours, (ii) across-track velocity contours and (iii) along-track velocity contours. Note the low Richardson numbers just above the fast outflow core.

smooth and it should be remembered that our velocity profiles are an average of an up and down cast, which could have time differences of up to an hour.

The results show that low Richardson numbers are located in the high velocity shear regions just above the fast flowing overflow core. There are regions where the Richardson number does go below one and even close to zero on a few occasions. This could provide evidence that mixing is taking place within these regions. The regions in section P where Richardson numbers are below 3, also coincide with those stations where we found Froude numbers greater than 1.

A stability analysis performed by Borenas and Lundberg (1988), for the May 1983 measurements, in high shear/velocity regions near our Faroe Bank Channel section show that the high stratification regions are barely able to suppress turbulence with Richardson numbers in the range 0.12–1.89. We see quite low Richardson numbers in our Faroe Bank Channel section in the region just above the outflow plume

on the southern side (not shown). Our  $Ri$  values from 1–7 around 550–600 m certainly fall within the range provided by Saunders (1990).

In conclusion, we find significant entrainment occurring immediately downstream of the Faroe Bank Channel sill in locations centred on the path of the outflow plume. Streamtube models have been used to model the deep-water plume through the Faroe Bank Channel (Price and Baringer, 1994; Lindblad, 1997). Lindblad (1997) developed a streamtube model based on previous studies but included a slight modification to include stability effects in the turbulent entrainment parameterisation via the bulk Froude number. This modification did not change the results of his model, which resulted in an underestimate of the amount of entrainment taking place. The suggested reason for the lack of entrainment was the lack of a parameterisation being included for the broadening of the plume downstream, which was included in the Price and Baringer (1994) study in terms of the Ekman number. However, they discovered that Froude numbers remain less than one until the outflow reaches just east of Iceland approximately 250–300 km downstream from the sill. This is in conflict with our observations and previous observations (Borenas and Lundberg, 1988; Saunders, 1990), which indicate entrainment occurring much earlier in the plume's path along the Iceland–Faroe ridge.

#### 4. Conclusion

While the cold, dense Faroe Bank Channel overflow is confined by bathymetry in sections FBC and P, it spreads horizontally and deepens with increasing distance from the sill. The overflow follows the isobaths in confined regions of the channel, but shows a significant down slope flow in sections Q and S. In line with previous transport estimates, such as Saunders (1990) estimate of  $1.9 \pm 0.4$  Sv for water  $< 3$  °C, we find 1.6 Sv of transport below 3 °C for the 5 days period when we made observations.

High friction estimates are made in the overflow where there were high velocities and deep bottom mixed layers. Our friction analysis is based on the velocity spirals observed, due to Ekman flow, particularly in the fast flowing stations. Bottom friction estimates can also be made in the constant stress layer just above the bottom (Girton et al., 2001). The constant stress layer would appear in velocity profiles over a small vertical extent, approximately 10 m, near the bottom, which has the same bearing as the principal orientation. However, there was little evidence of a constant stress layer in the LADCP velocity profiles, perhaps due to uncertainty in how closely we were able to observe velocity towards the bottom. Despite this, our stress values compare well with Johnson and Sanford (1992) who found a logarithmic layer in the bottom 30 m at the Faroe Bank Sill and obtained the stress value  $3.5 \pm 1.3$  Pa.

Our estimates of the drag coefficient of  $0.5 \times 10^{-3}$  are about a factor of five smaller than standard predictions. One major difference between our results (Table 1) and those of

Armi (1977) relates to the relative depths of the Ekman layer to the mixed layer height. Armi (1977) stated that the mixed layer is always approximately six times larger than the Ekman layer height. However, our results indicate comparable Ekman layer and mixed layer heights with the Ekman layer generally a bit thicker than the mixed layer. This difference may be due to the fast flowing plume over a sloping bottom in contrast to the quiescent abyssal boundary layers analysed by Armi.

Estimating turbulent diffusivities is our preferred method for looking at mixing. As our measurements are not instantaneous in time, and did not therefore catch instant states of the velocity shear and stratification, the Richardson number estimates are questionable. The pattern of Richardson numbers indicates where mixing may be occurring, a pattern that agrees well with the Froude number estimates at section P. Mixing and entrainment are an order of magnitude larger in the first 10 km downstream of the sill than over the next 40 km.

### Acknowledgements

The authors would like to thank all those who participated on *Discovery* cruise 242. We also thank Peter Saunders for discussions on diffusivity calculations and Andy Hogg for his perspective on mixing. This work was funded by NERC as part of the James Rennell Division's core strategic project 'Large scale long term ocean circulation'.

### References

- Armi, L., 1977. The dynamics of the bottom boundary layer of the deep ocean. In: Nihoul, J.C.J. (Ed.), *Bottom Turbulence*, Proceedings of the 8<sup>th</sup> International Liège Colloq. on Ocean Hydrodynamics (Elsevier Oceanography Series, 19). Elsevier Scientific Publishing Company, pp. 153–164.
- Baines, P.G., 2001. Mixing in flows down gentle slopes into stratified environments. *J. Fluid Mech.* 443, 237–270.
- Baringer, M.O., Price, J., 1997a. Mixing and spreading of the Mediterranean outflow. *J. Phys. Oceanogr.* 27, 1654–1677.
- Baringer, M.O., Price, J., 1997b. Momentum and energy balance of the Mediterranean outflow. *J. Phys. Oceanogr.* 27, 1678–1692.
- Borenas, K.M., Lundberg, P.A., 1988. On the deep-water flow through the Faroe Bank Channel. *J. Geophys. Res.* 93, 1281–1292.
- Cunningham, S.A., 2000. Atlantic–Norwegian Exchanges, RRS *Discovery*. 242 SOC Cruise Report No. 28, 242, 128 p.
- Duncan, L.M., Cunningham, S.A., Bryden, H.L., 2002. Physical data from the Faroe Bank Channel overflow experiment collected on RRS *Discovery* Cruise 242, 7 September–6 October 1999 SOC Internal Report No. 79.
- Girton, J.B., Sanford, T.B., Käse, R.H., 2001. Synoptic sections of the Denmark Strait overflow. *Geophys. Res. Lett.* 28, 1619–1622.
- Hansen, B., Østerhus, S., 2000. North Atlantic–Nordic Seas exchanges. *Prog. Oceanogr.* 45, 109–208.
- Hansen, B., Turrell, W.R., Østerhus, S., 2001. Decreasing overflow from the Nordic seas into the Atlantic Ocean through the Faroe Bank Channel since 1950. *Nature* 411, 927–930.
- Høyer, J.L., Quadfasel, D., 2001. Detection of deep overflows with satellite altimetry. *Geophys. Res. Lett.* 28, 1611–1614.
- Johnson, G.C., Sanford, T.B., 1992. Secondary circulation in the Faroe Bank Channel outflow. *J. Phys. Oceanogr.* 22, 927–933.
- Killworth, P.D., 2001. On the rate of descent of overflows. *J. Geophys. Res.* 106, 22267–22275.
- Lindblad, K., 1997. Near-source behaviour of the Faroe Bank Channel deep-water plume. Göteborg University, Department of Oceanography, Göteborg, Sweden 41 p.
- Price, J.F., Baringer, M.O., 1994. Outflows and deep water production by marginal seas. *Prog. Oceanogr.* 33, 161–200.
- Saunders, P.M., 1990. Cold outflow from the Faroe Bank Channel. *J. Phys. Oceanogr.* 20, 29–43.
- Saunders, P.M., 2001. The dense northern overflows. In: Siedler, G., Church, J., Gould, J. (Eds.), *Ocean Circulation and Climate: Observing and Modelling the Global Ocean*. (International Geophysics Series No. 77). Academic Press, San Diego, CA, pp. 401–417.
- Smith, W.H.F., Sandwell, D.T., 1997. Global sea floor topography from satellite altimetry and ship depth soundings. *Science* 277, 1956–1962.